Published in final edited form as:
Methods Enzymol. 2009 ; 469: 303–328. doi:10.1016/S0076-6879(09)69015-7.

STUDYING RNA USING SITE-DIRECTED SPIN-LABELING AND CONTINUOUS-WAVE ELECTRON PARAMAGNETIC RESONANCE SPECTROSCOPY

Xiaojun Zhang[*], **Pavol Cekan**[†], **Snorri Th. Sigurdsson**[†], and **Peter Z. Qin**[*]

[*]Department of Chemistry, University of Southern California, Los Angeles, California, USA
[†]Department of Chemistry, Science Institute, University of Iceland, Reykjavik, Iceland

Abstract

In site-directed spin-labeling (SDSL), a stable nitroxide radical is attached to a specific location within a macromolecule and electron paramagnetic resonance (EPR) spectroscopy is used to interrogate the local environment surrounding the nitroxide. The SDSL strategy enables probing site-specific structural and dynamic features of RNA in solution without being limited by the size of the molecule, thus serving as a unique tool in biophysical studies of RNA. This chapter describes the use of continuous-wave (cw)-EPR to study dynamic features of RNAs as well as to monitor interactions between them. Various approaches for attaching nitroxide spin labels to nucleic acids are described, followed by detailed descriptions of cw-EPR spectral acquisition and processing procedures. Specific examples are subsequently used to illustrate analysis of EPR spectra, showing how information regarding the parent RNA can be extracted.

Information about RNA structure and movement is critical for our understanding of how RNA is able to carry out its multifaceted functions. One spectroscopic technique that has shown great promise to study RNA, as well as other biopolymers, is electron paramagnetic resonance (EPR) spectroscopy, also named electron spin resonance (ESR) spectroscopy. EPR is a magnetic resonance technique that monitors the behaviors of unpaired electrons, and has long been used to study structure and dynamics of biomolecules (see recent reviews by Klug and Feix, 2008; Sowa and Qin, 2008). Structural information can be obtained by distance measurements, that is, by determination of distances between two spin-centers, and is the topic of another chapter in this volume (see Chapter 16 in this volume).

This chapter focuses on continuous-wave (cw)-EPR, which has been commonly used for studying dynamic features and interactions between biomolecules. The technique is capable of covering motions ranging from picosecond (ps) to millisecond (ms). Other advantages of EPR are that small amount of material (typically 0.05–1.0 nmol) is required, samples are not limited by molecular size, and the measurements can be carried out under physiological conditions. However, RNA does not contain stable unpaired electrons and, therefore, spin-centers must be introduced into the RNA in order to conduct EPR studies.

This chapter first summarizes methods for attaching spin labels to nucleic acids, with a special focus on RNA (Section 1). Detailed protocols for these labeling methods have been described in a series of recent publications (Edwards and Sigurdsson, 2007; Qin *et al*., 2007; Schiemann *et al*., 2007), and will not be repeated here. Acquisition and processing of cw-EPR spectrum will then be described in detail (Section 2), followed by a brief discussion of spectral analysis (Section 3). Specific examples of using cw-EPR to study dynamics and interactions in RNA will subsequently be given (Section 4).

1. SITE-DIRECTED SPIN-LABELING

Since RNA is diamagnetic, EPR studies of RNA require incorporation of unpaired electrons into the biopolymer. Nitroxides in five- or six-membered rings that are flanked by methyl groups are stable organic free radicals that are commonly used for spin-labeling (Fig. 15.1). For a free radical, the nitroxide is chemically unusually stable because the unpaired electron is shared by the nitrogen and the oxygen atoms. The radical is also sterically protected from reaction with solvent and other molecules by the methyl groups.

The labeling must be specific, that is, directed to a specific site in the RNA to yield meaningful results pertaining to specific nucleotides. This is commonly referred to as site-directed spin-labeling (SDSL) (Altenbach *et al.*, 1989; Barhate *et al.*, 2007; Edwards *et al.*, 2001; Kim *et al.*, 2004; Qin *et al.*, 2001, 2003; Schiemann *et al.*, 2004). Therefore, incorporation of multiple labels through enzymatic RNA synthesis (e.g., triphosphate poly-merization with polymerases; Keyes *et al.*, 1997) is of limited value. Instead, labels are generally introduced chemically, either during chemical synthesis of the nucleic acid or by postsynthetic modification of the polymer.

After selecting a specific nucleotide (or nucleotides for multiple labels) for spin-labeling in the RNA of interest, the point of attachment is chosen. The label can be incorporated into the base (Barhate *et al.*, 2007; Fischhaber *et al.*, 1997; Keyes *et al.*, 1997; Piton *et al.*, 2007; Prisner *et al.*, 2001;Qin *et al.*, 2003; Schiemann *et al.*, 2004; Spaltenstein *et al.*, 1988), sugar (Edwards *et al.*, 2001; Kim *et al.*, 2004), or the phosphodiester (Fidanza *et al.*, 1992; Nagahara *et al.*, 1992; Qin *et al.*, 2001) (Figs. 15.2 and 15.3). In addition, the structure of the label needs to be taken into consideration. For example, if spin labels are linked to the RNA with a flexible linker, the nitroxide ring may have considerable motions independent of the parent nucleic acid, which must be accounted for during data analysis. Excess linker flexibility may give rise to difficulties in detecting nucleic acid dynamics or measuring interspin distances. As with all chemical modifications of RNA, spin-labeling may interfere with the structure and function of the nucleic acid. Therefore, one must carefully evaluate the effect of the label itself by running appropriate control experiments.

1.1. Spin-labeling during chemical synthesis of the nucleic acid

Nucleic acids are synthesized chemically in laboratories around the world using automated synthesizers. Therefore, if one can prepare a phosphoramidite of a spin-labeled nucleoside, which is the building block for oligonucleotide synthesis, the spin label can be incorporated into any sequence and at any site in the sequence. Many different spin-labeled nucleosides have been prepared, some of which are shown in Fig. 15.2, and incorporated into nucleic acids. For example, spin labels have been attached to the exocyclic amino groups of C (**1**) and A (**2**), the 2-position of A (**3**), and the 5-position of pyrimidines (**4**–**6**). The most important advantage of this approach over the postsynthetic method described below is that it enables incorporation of spin label modifications that require an elaborate synthetic effort, such as C-nucleosides (**7**) (Miller *et al.*, 1995) and the rigid spin label Ç (**8**) (Barhate *et al.*, 2007).

The drawbacks of the synthetic approach include the effort in preparation of the spin-labeled phosphoramidites and exposure of the spin label to the conditions of the chemical synthesis. The latter also applies for methods that use on-column modification during the synthesis (Piton *et al.*, 2007; Schiemann *et al.*, 2004). For example, the iodine solution that is commonly used for the phosphorous oxidation during the synthesis reduces nitroxides (Cekan *et al.*, 2008; Gannett *et al.*, 2002; Piton *et al.*, 2007), although this problem can be circumvented by using *tert*-butyl hydroperoxide (Cekan *et al.*, 2008). Partial decomposition of nitroxides is also observed due to the acid treatment that is used to remove the dimethoxytrityl protecting groups

during the synthesis cycle (Abakumov and Tikhonov, 1969; Cekan *et al.*, 2008; Piton *et al.*, 2007).

1.2. Postsynthetic spin-labeling

Chemical synthesis of RNA is more challenging than for DNA, due to the presence of the 2′-hydroxyl group, which needs to be protected during oligomer synthesis and subsequently deprotected. Thus, postsynthetic labeling has been more extensively used for the preparation of spin-labeled RNA. In this approach, the nucleic acid is first synthesized and subsequently incubated with a spin-labeling reagent. To ensure site-specific labeling, the RNA must contain a reactive group that can be specifically modified with the labeling reagent. Such modified RNAs and spin-labeling reagents are in many cases commercially available. Therefore, scientists who do not have extensive training in organic synthesis can readily prepare spin-labeled oligomers with the postsynthetic method. Another advantage of postsynthetic labeling is that the spin label is not subjected to the reagents used in oligomer synthesis, thus avoiding partial reduction of the nitroxide.

Incorporation of spin labels through chemical synthesis of the nucleic acid has focused on spin-labeled nucleobases. On the other hand, postsynthetic labeling has been used for attaching nitroxides to different parts of nucleotides: at nucleoside bases (Fig. 15.3A) (Hara *et al.*, 1970; Okamoto *et al.*, 2004; Qin *et al.*, 2003; Varani *et al.*, 1999), sugars (Fig. 15.3B) (Edwards *et al.*, 2001; Kim *et al.*, 2004), and the internal phosphate backbone (Fig. 15.3C) (Fidanza *et al.*, 1992; Nagahara *et al.*, 1992; Qin *et al.*, 2001). Spin labels have been attached to the 5′-end of RNA by modification of a 5′-phosphorothioate (**15**, **16**, Fig. 15.3D) (Grant *et al.*, 2008; Macosko *et al.*, 1999) and the 3′-end by periodite oxidation and reductive amination (**17**, Fig. 15.3D) (Hermann, 1977). However, the most general spin-labeling approach is incorporation of nitroxides at internal sites of the oligomer (Fig. 15.3A–C), which has been used extensively to prepare spin-labeled RNA. For example, incorporation of 2′-amino groups at selected nucleotides enables selective reaction with aliphatic isocyanates, resulting in 2′-urea-slabeled oligomers (Fig. 15.4A) (Edwards *et al.*, 2001). The reactivity of sulfur atoms has also been utilized for postsynthetic labeling of pyrimidine bases (Fig. 15.4B) (Qin *et al.*, 2003) and at the phosphodiester (Fig. 15.4C) (Qin *et al.*, 2001).

2. ACQUISITION AND PROCESSING OF cw-EPR SPECTRUM

A typical layout of an EPR spectrometer is shown in Fig. 15.5. While the general principles of operation and detection are the same for different spectrometers, specific steps may vary. The readers are encouraged to consult the manual and vendor regarding each individual spectrometer. Examples used in discussions below are based on a Bruker EMX X-band spectrometer that is equipped with an ER-041X microwave bridge and a high-sensitivity cavity (ER-4119HS, Bruker Biospin, Inc.).

There are four general steps in acquiring an undistorted cw-EPR spectrum with the desired signal-to-noise ratio (S/N): (1) sample preparation and insertion; (2) cavity coupling; (3) spectral acquisition; and (4) spectral processing. Depending on the spectral line-shape, one may be able to obtain a cw-EPR spectrum with a sufficient S/N in less than 15 minutes using as low as 50 pmol of nitroxide-labeled samples. Data averaging, typically in the order of tens of minutes to hours, can be used to measure weaker signals.

2.1. Sample preparation and insertion

The required total number of spins in a measurement is typically 10^{13}–10^{14}, which translates into ~ 100 pmol of nitroxide. Biological samples are usually prepared in buffer solutions, and it is important to ensure that no undesired EPR signal comes from the buffer. For nitroxide-

labeled samples, diamagnetic (EPR silent) metal ions (e.g., K^+, Na^+, Mg^{2+}, Ca^{2+}) are acceptable. Paramagnetic metal ions, such as Cu^{2+}, Fe^{2+}, Mn^{2+}, have EPR signals and thus may interfere with SDSL studies. In addition, compounds such as sucrose, glycerol, or ficoll are often added to solution to increase solvent viscosity and reduce the overall rotational tumbling motion of the macromolecular (*vide infra*). They may also serve as cryoprotecting agents to ensure a glass-like homogeneous mixture when measuring frozen samples.

EPR samples are held in glass or quartz capillaries/cells. Glass is much cheaper than quartz, and often sufficient for cw-EPR measurements. However, glass typically gives a much more prominent background signal at low temperature due to the presence of impurities (e.g., defects or paramagnetic metal ions). EPR capillaries/cells vary in size and shape depending on the resonator used with the spectrometer. They are chosen to place the sample at the "active" volume of the resonator (usually at the center), where the magnetic field is at its maximum and the electric field is at the minimum.

To obtain an optimal signal, the sample should fill the resonator active volume as much as possible. This dictates the sample volume and the positioning of the capillary/cell in the cavity. For example, with the Bruker high-sensitivity cavity, a tilted capillary covers a smaller fraction of the active volume and therefore reduces signal intensity. It should be noted that water absorbs microwave radiations via interacting with the electric field, thus lowering the cavity *Q* value and making it difficult or impossible to tune. Therefore, aqueous samples, which include almost all RNA samples, tend to be "lossy" with low *Q* values. This may restrict the size of the capillaries/cells and the sample volume.

2.2. Critical coupling of cavity

After sample insertion, the cavity is "tuned" to achieve critical coupling, so that the microwave power stored in the cavity is maximized while its dissipation is minimized. Tuning generally involves two steps: "rough-tuning" to approximately match the microwave frequency to the cavity resonance frequency; followed by "fine-tuning" to establish critical coupling.

In rough-tuning, the spectrometer is put at the "tune" mode. A low microwave power (e.g., 25 dB, 0.63 mW) is applied to generate the "model pattern", which is the microwave power reflected from the resonator as a function of the microwave frequency. Microwave frequency is adjusted to position the "dip", which reports the frequency at which the microwave power is absorbed, at the center of the model pattern. This indicates an approximate match between the microwave frequency and the cavity resonance frequency. The resonator is then further adjusted (e.g., move the iris and/or change the "signal phase" if using a Bruker EMX system) to make the dip symmetrical and as deep as possible (maximal power absorbed). One should also allow the cavity and sample to come to thermal equilibrium during rough-tuning in order to minimize drifts in later fine-tuning.

To fine-tune the cavity, the spectrometer is put in the "operate" mode. Adjust the microwave frequency, the iris position (resonator parameter), and the reference arm current ("bias") so that the analog indicators for the automatic frequency control ("AFC") and the "diode" always stay at the center as the microwave power is increased from minimum (e.g., 50 dB, 2 μW) to maximum (e.g., 0 dB, 200 mW). This indicates that at all power levels, the majority of microwave power is stored in the resonator and very little is reflected. Adjust the "signal phase" to let the "diode" indicator reach the maximum, and then decrease the "bias" if necessary to put "diode" back to center again.

2.3. Spectral acquisition

After cavity tuning, acquisition parameters need to be set up before acquiring a spectrum. Table 15.1 lists these parameters together with example values used for acquiring a nitroxide spectrum on a Bruker EMX system. These values vary significantly depending on the spectrometer, the resonator, and the sample, and thus should be optimized in each individual case. Improper acquisition parameters lead to low quality spectra, with the two major symptoms being: (1) no signal or very weak signal; and (2) spectral distortion. These pitfalls and their remedies are discussed in the following sections.

2.3.1. No signal or very small signal—If sufficient amount of spins (>10^{13} for nitroxide-labeled sample) is present but no signal or very weak signal is detected, one should check the following parameters.

2.3.1.1. Sample positioning: The capillary/cell should be straight and not tilted, with the sample occupying the resonator active volume (e.g., cavity center). To ensure proper sample positioning, one can insert the sample with the spectrometer set at the "tune" mode, and adjust the capillary so that the dip displacement is maximized.

2.3.1.2. Center field and scan width: These two parameters dictate the center and the width of the measured spectrum, and should be set to cover the entire region of all desired signals. For nitroxides, the splitting of peaks can be up to ~ 70 Gauss (G), and most studies use a convenient scan width of 100 G.

The center field is related to the resonating microwave frequency according to

$$H=\frac{h\nu}{g\beta_e} \tag{15.1}$$

where h is the Planck constant ($h = 6.626 \times 10^{-34}$ J s), ν is the microwave frequency, β_e is the Bohr magneton (the intrinsic unit of an electron magnetic moment, $\beta_e = 9.274 \times 10^{-24}$ J/T), and g is the electron spin g-factor. The nitroxide g-factor is very close to that of a free electron ($g_e \sim 2.0023$), and Eq. (15.1) can be rewritten as:

$$H=356.8\nu \tag{15.2}$$

where H is expressed in Gauss, and ν in 10^9 Hz (GHz). For a microwave frequency of 9.5 GHz (X-band), the corresponding magnetic field is 3390 G.

2.3.1.3. Modulation phase: EPR signal is detected using phase-sensitive lock-in amplification (Blair and Sydenham, 1975; Cova *et al.*, 1979; Poole, 1996), and therefore depends on the cosine of the phase angle (phase difference) between a reference signal and the modulated EPR signal. The parameter "modulation phase" is a phase shifter that changes the phase of reference signal in order to optimize detection of the desired EPR signal. For cw-EPR, the in-phase signal is detected, with the phase shifter adjusted to give a phase angle of 0° (maximal EPR signal). To determine the proper modulation phase, one can measure a sample with a varying modulation phase. The minimal signal corresponds to the out-of-phase position (phase angle = 90° or 270°) from which the in-phase value can be deduced by subtracting (or adding) 90°.

2.3.1.4. Receiver gain: Sufficient receiver gain is required for observing the signal. However, a high receiver gain does not improve S/N, as noises are amplified to the same degree as the

signal. One should also avoid excessive receiver gain to prevent "clipping" of the spectrum (signal outside of maximal detection range).

2.3.1.5. Number of scans (signal averaging): EPR S/N is proportional to the square root of number of scans. In theory, a desirable S/N can always be achieved by increasing the number of scans. In practice, however, over a prolonged period, system instability (temperature variations, air drift, etc.) and background signals (e.g., impurities at capillary and/or resonator) may give a baseline with variable features. Therefore, very weak signals may not be detectable even with a very large number of scans.

2.3.2. Spectral distortion—The line-shape of a true (undistorted) EPR spectrum should be independent of the acquisition parameters, and therefore to assess spectral distortion one can compare spectra acquired with different parameters. Figure 15.6 illustrates the effect of modulation amplitude on EPR line-shape. The central line-width (peak-to-peak width ΔH_{pp} = 1.6 G) remains unchanged when the modulation amplitude is increased from 0.5 to 1 G; while at a modulation amplitude of 10 G, distortion and line-broadening (ΔH_{pp} = 6.4 G) can be clearly observed. The main sources of spectral distortions are modulation amplitude, microwave power, and scanning rate (speed). These are discussed in the following sections.

2.3.2.1. Modulation amplitude and modulation frequency: High modulation amplitude increases EPR signals intensity, but may also distort the line-shape (Fig. 15.6). It is advised to use a modulation amplitude that is approximately equal to the line-width (ΔH_{pp}) of the narrowest peak one tries to resolve. This amounts to 1–2 G for most nitroxide systems. Moreover, a modulation frequency of 100 kHz is typically used.

2.3.2.2. Microwave power: A microwave power of ~ 2 mW (20 dB) is typically used to acquire a nitroxide spectrum. Without saturation, EPR signal is proportional to the square root of the microwave power. As microwave power increases, the rate of excitation may become greater than the rate of relaxation. This decreases the difference in spin populations between the ground state and the excited state, thus reducing the EPR signal. High power may also cause line-broadening (Fajer, 2000).

2.3.2.3. Scanning speed: Number of points, conversion time, and time constant: A greater number of points in a spectrum gives better resolution, but requires longer sweep time. A general rule is to have at least 10 points for the narrowest line in a spectrum. "Conversion time" is the amount of time the detector spends integrating at one field position before moving to next one, and "time constant" is a measure of the cutoff frequency of the lock-in detector, which will filter out signals (noises) with frequencies greater than 1/(time constant). The time constant is generally kept below the conversion time to prevent spectral distortion, although for weak signal a long time constant may be used. Conversion time should be sufficiently long to ensure that a weak signal is captured during the digitization steps. However, lengthy conversion time may lead to a prolonged sweep time (sweep time = conversation time × number of points) and may cause baseline drift. One may avoid this by acquiring more scans with short conversion time. In doing so, the baseline drift may only cause a constant offset, which will not distort the spectrum.

2.4. Spectral processing

After acquisition of the spectral data, a number of processing steps, including spectrum averaging, baseline correction, and spectrum integration, are executed to prepare the spectrum for further analysis. These steps can be carried out using software provided by the vendor (e.g., WinEPR from Bruker). The spectrum can also be exported using the "ASCII" format, then processed and analyzed using customized programs relying on commercially available

software, such as Microsoft Excel, Matlab, or Labview. The general ideas behind each processing step, illustrated using examples generated with Microsoft Excel, are discussed in the following sections.

2.4.1. Spectrum averaging—Spectrum averaging is probably the most effective way to increase S/N (Fig. 15.7), and is particularly important when measuring spectrum with broad lines.

2.4.2. Baseline correction—An ideal baseline should be completely straight without any feature. This may not be the case, especially for samples with weak signals, due to a number of reasons. The cavity, the cryostat, or the capillary/cell may have a small amount of contamination, the signal of which may be reduced or even eliminated by cleaning. In addition, system instability (temperature variations, air drift, etc.) may also yield broad features in the baseline.

One may acquire a "background spectrum" and then subtract it from the averaged experimental signal (Fig. 15.7). In doing so, the control should resemble the real sample as much as possible: use the same buffer and the same exact type of capillary; insert to the same position of the cavity; and performing the scan immediately after sample measurement with the same parameters. A reasonably reproducible background spectrum can be obtained in many cases. In extreme situations (e.g., large variations in background signal due to capillary changes), one might have to quench the EPR signal *in situ* (e.g., injecting ascorbic acid to reduce the nitroxide) to obtain the background spectrum.

2.4.3. Spectral integration—With the use of lock-in detection, the measured EPR signal corresponds to the first derivative of the radical absorption spectrum. The 1st integral of a measured EPR spectrum as a function of the magnetic field is computed according to

$$Y(H_{\mathrm{i}})=\sum_{j=1}^{n_{\mathrm{i}}} y_j \Delta H \tag{15.3}$$

with

$$n_{\mathrm{i}}=\frac{H_{\mathrm{i}}-H_{\mathrm{b}}}{\Delta H} \tag{15.3a}$$

in the calculations, y_j is the amplitude of the detected EPR signal at magnetic field H_j, ΔH is a fixed interval (e.g., ΔH = 1 G; smaller ΔH gives more precise integral), and n_{i} is the number of intervals between the beginning of the spectrum (H_{b}) and the current field position (H_{i}). The 1st integral (Y_{i} vs. H_{i}) gives the absorption spectrum (Fig. 15.8A).

The 1st integral can be integrated again to give the area under the absorption spectrum between H_{b} and H_{i}:

$$\mathrm{Area}(H_{\mathrm{i}})=\sum_{j=1}^{n_{\mathrm{i}}} Y_j \Delta H \tag{15.4}$$

The 2nd integral (designated as A) generally refers to the area computed over the entire spectrum ($n = (H_{\mathrm{f}} - H_{\mathrm{b}})/\Delta H$, with H_{f} being the magnetic field at the end point of the spectrum), and is directly proportional to the total number of spins (Fig. 15.8A). It should be noted that

the actual value of the 2nd integral is affected significantly by the baseline, and therefore is meaningful only if the baseline is acceptable or has been corrected. The 1st and 2nd integrals are used in a number of processing steps described in the following sections.

2.4.3.1. Baseline corrections: With an ideal baseline, the 1st integral should be completely flat in the outer low-field and high-field regions (Fig. 15.8A). Therefore, the 1st integral can be used in baseline correction, with the rules of thumb in selecting the correct baseline being that: (i) no negative regions in the 1st integral (absorption spectrum); and (ii) low-field and high-field regions beyond the absorption peaks are flat and equals to 0.

2.4.3.2. Spectral normalization: Many spectral analysis procedures compare spectrum per spin, therefore the measured spectrum has to be normalized (Fig. 15.8B). Normalization is carried out by dividing the measured spectrum by its 2nd integral, which is proportional to the total number of spins.

2.4.3.3. Spin counting: While the 2nd integral reports the total number of spins, the proportional constant depends on acquisition parameters and the specific spectrometer. To obtain the proportional constant, one can generate a calibration curve, where samples with known amount of spins are measured (Fig. 15.8C). Spin counting generally yields a “spin concentration”, which is proportional to the total number of spins as the spectrometer activity volume is considered constant. An important reason for spin counting is to assess labeling efficiency, which is the ratio of the spin concentration to that of the RNA (e.g., determined by UV–Vis absorption measurement, Fig. 15.8C).

3. SPECTRAL ANALYSIS

The line-shape of a cw-EPR spectrum is dictated by the reorientation dynamics (motions) of the nitroxide, which average the anisotropic nitroxide magnetic tensors. Figure 15.9A shows simulated X-band EPR spectra of a nitroxide undergoing isotropic tumbling, with the nitroxide motion characterized by a rotational correlation time τ. As nitroxide motions reduce (longer τ), the EPR spectrum shows broader lines, and extra features appear at the low-field and high-field regions.

The goal of assessing nitroxide dynamics is to obtain information at the labeling sites of the macromolecule. In SDSL studies, the macromolecule may influence nitroxide dynamics via a combination of three modes (Fig. 15.9B): (i) the overall rotational motion of the macromolecule (characterized by a rotational correlation time τ_R); (ii) torsional rotations about bonds that connect the nitroxide ring to the macromolecule (τ_i); and (iii) segmental motions of the macromolecule at or near the labeling point (τ_B). The τ_i and τ_B motions may be influenced by site-specific macromolecular structural and dynamic features, while the τ_R motion is uniform across the macromolecule, and depends on the molecular size (weight) as well as solvent viscosity. As demonstrated by the examples of application, either τ_i/τ_B (example 1) or τ_R (example 2) effects can be used to study RNA.

A number of methods have been developed for assessing nitroxide dynamics based on the cw-EPR spectrum (see review by Sowa and Qin, 2008). In the semiquantitative approach, parameters measured directly from the EPR spectrum, such as the central line-width (ΔH_{pp}, Fig. 15.9A), the splitting of the resolved hyperfine extrema ($2A_{eff}$, Fig. 15.9A), and the second moment (H_2, characterizing how broad the spectrum is), are used to characterize nitroxide dynamics (Columbus and Hubbell, 2002, 2004; Mchaourab *et al.*, 1996). These parameters report on the nitroxide mobility, which describes a combined effect of the rate and the amplitude of motion. For example, a broad center line gives a small $(\Delta H_{pp})^{-1}$ value and indicates low mobility, which can result from low frequency but large amplitude motions, or small amplitude

motions with fast rates. The line-shape parameters can be easily measured on a properly processed EPR spectrum, and provide a means to quickly access relative nitroxide mobility at different sites. This approach, specifically by measuring $2A_{eff}$, was used in example 1 to probe site-specific dynamic features of the HIV TAR RNA.

In addition to the semiquantitative approach, more quantitative analytical approaches have been reported. For example, in the fast motion regime ($\tau \sim 10^{-11}$–10^{-} s at X-band), one can compute the nitroxide rotational correlation time based on the measured line-widths and amplitudes (Marsh, 1981; Qin *et al.*, 2001; Xi *et al.*, 2008). Furthermore, it is possible to simulate a nitroxide spectrum based on quantum mechanics and specific motional models (Columbus *et al.*, 2001; Grant *et al.*, 2009; Hustedt *et al.*, 1993; Liang *et al.*, 2000; Qin *et al.*, 2006; Schneider and Freed, 1989). The details of these advanced analysis techniques are not discussed here, interested readers are instead referred to a recent review (Sowa and Qin, 2008) and the relevant literatures.

4. EXAMPLES OF APPLICATION

4.1. Example 1: cw-EPR studies of the HIV TAR RNA

4.1.1. Variable dynamic signatures in ligand-bound TAR RNA—The trans-activation response (TAR) RNA is a structural motif at the 5′-end of the HIV RNA, which interacts with the Tat protein during HIV transcription. The binding site of the Tat protein is an internal loop in the TAR RNA (Fig. 15.10A). The TAR–Tat interaction assures an efficient transcription and thereby facilitates replication of the HIV virus (Frankel, 1992). Therefore, interference with the TAR–Tat interaction has been pursued as a strategy to combat HIV. Below is a description of how cw-EPR spectroscopy has yielded information about RNA dynamics that are correlated with the structure of the TAR RNA receptor bound to various ligands.

Four spin-labeled TAR RNAs were prepared using the 2′-labeling strategy described in Fig. 15.4A, each RNA having one spin label in the 2′-position position of either U23, U25, U38, or U40 (Fig. 15.10A) (Edwards *et al.*, 2001). Using the width of the X-band EPR spectra ($2A_{eff}$) as a measure of mobility (Fig. 15.10B), it became clear that U23 and U25 had similar mobility, which was faster than that observed for U38 and U40. This was consistent with the fact that U23 and U25 were located in a flexible loop and showed that the spin label was a good reporter of the mobility of nucleotide to which it was attached (Edwards *et al.*, 2001). Thus, these results encouraged investigation of the changes in dynamics of individual nucleotides in the TAR RNA upon ligand binding.

The effects of several ligands, such as metal ions (Edwards and Sigurdsson, 2003; Edwards *et al.*, 2002), small organic molecules (Edwards and Sigurdsson, 2002), and peptides (Edwards *et al.*, 2002, 2005) on TAR RNA dynamics were studied by EPR. The EPR data were analyzed by plotting the change in the spectral width ($2A_{eff}$) upon ligand binding as a function of spin label position, which gives a dynamic signature for each ligand (Fig. 15.10C). The dynamic signatures are very sensitive to the structure of ligand–receptor complex; of the six examples shown, no two are alike. The first three dynamic signatures are representatives of three classes of metal ions observed when studying the binding of 10 different metal ions to the TAR RNA (Edwards and Sigurdsson, 2003). Not much change is observed in the spectral width for Li^{+}, whereas a large narrowing of the spectral width for U25 and U40 was observed for Mg^{2+} binding to the TAR RNA. The fact that Na^{+} and Mg^{2+} show different dynamic signatures (a large difference in the spectral width of U25) indicates that the two structures are different, which has been verified by NMR spectroscopy (Al-Hashimi *et al.*, 2003).

The latter three dynamic signatures in Fig. 15.10C are those of small molecules that have been found to inhibit the TAR–Tat interaction (Edwards and Sigurdsson, 2002). Each one of these

molecules has been shown to bind to the TAR RNA in a different manner and all give different dynamic signatures. Therefore, determination of dynamic signatures by cw-EPR spectroscopy can readily identify binding sites in RNA and should be useful for screening libraries of ligands for binding to specific sites in drug-discovery programs.

4.1.2. Dynamic signatures and structural requirements in the TAR–Tat interaction—

Given the sensitivity of dynamic signatures for the structure of ligands binding to the TAR RNA, this approach was applied to study the interaction of the TAR RNA with its biological partner, the Tat protein. The Tat protein is ca. 86 residues long, but a short peptide spanning this region, YGRKK**R**^{52}RQRRR (Tat 47–58), binds to the TAR RNA with high affinity (dissociation constant K_d ~ 200 n*M*) (Hamy *et al.*, 1993; Roy *et al.*, 1990). Arginine 52 (R52) has been identified as an essential amino acid for the TAR–Tat interaction. Although the NMR structure of the TAR RNA bound to a peptide has not been solved, a high-resolution NMR structure is available for argininamide, which is the simplest analog of the Tat protein, complexed with the TAR RNA (Brodsky and Williamson, 1997). Figure 15.11A shows dynamic signatures for argininamide, the Tat wild-type peptide (YGRKK**R**^{52}RQRRR) and a Tat mutant peptide (YKKKK**R**^{52}KKKKA). The mutant peptide has been shown to bind to the TAR RNA with similar affinity as the wild-type sequence (Edwards *et al.*, 2002). The three ligands have similar dynamic signatures: U23, U38, and U40 have lower mobility, while U25 is faster than the unbound TAR RNA. This indicates a similar structural motif for all three complexes. There is, however, a striking difference between the mutant peptide and the wild type: an enormous reduction of mobility of U23 and U38 for the wild type. Interestingly, U23 and U38 are involved in formation of a triple base pair upon binding argininamide (Brodsky and Williamson, 1997). This indicates that amino acids flanking R52 in the wild-type sequence make specific contacts to the RNA, which greatly affects its internal motion.

To determine which amino acids promoted specific TAR–Tat complex formation, a series of peptide mutants were prepared and their dynamic signatures collected (Edwards *et al.*, 2005). Figure 15.11B shows the sequence of the peptides and the changes in spectral width for U38 upon binding the peptides. The data clearly show that amino acids flanking R52 at the carboxyl terminus participate in this specific interaction. In particular, the R56K mutant (Fig. 15.11B, second peptide from the bottom) shows a similar spectral width as argininamide, pointing to the importance of this amino acid in the formation of a specific complex. Inspection of the crystal structure of the Tat protein shows that R52 and R56 are the extremes of an apparent palm on the protein surface that is a likely binding site (Edwards *et al.*, 2005). Thus, information about the dynamics of nucleotides in the TAR RNA obtained by cw-EPR has enabled identification of specific structural requirements in the Tat protein and demonstrates the utility of EPR spectroscopy for investigating RNA-protein interactions.

4.2. Example 2: Studying RNA/RNA interactions via cw-EPR reported τ_R effects

The global tumbling of a 25 nucleotide (nt) oligonucleotide (~ 7500 Da) is estimated to have a τ_R of approximately 4 ns in aqueous solution at room temperature (Cantor and Schimmel, 1980; Qin *et al.*, 2003), which affects the X-band cw-EPR spectrum. In such cases, changes in the size of the system due to interactions with other macromolecules, such as a complimentary strand (Keyes and Bobst, 1998), a partner nucleic acid (Qin *et al.*, 2001), or a protein (Keyes and Bobst, 1998; Xi *et al.*, 2008; Zhang *et al.*, 2008), will change the EPR spectrum. Such spectroscopic changes provide a reporter to monitor the interactions. In the following example, the τ_R effect was used to study a frequently used RNA tertiary interaction motif—binding between a GAAA tetraloop and its RNA receptor (Qin *et al.*, 2001) (Fig. 15.12).

In this study, nitroxide label **14** (Fig. 15.3C) is attached near the 5′-terminus of a 12-nt RNA hairpin (TL1, Fig. 15.12A) containing the GAAA tetraloop (boxed region within TL1, Fig.

15.12A). TL1 spectra were obtained in a Mg^{2+} containing buffer with various concentrations of a 23-nt RNA (TLR, Fig. 15.12A) that includes the GAAA tetraloop receptor (boxed region within TLR, Fig. 15.12A). Line-broadening was observed when comparing spectra obtained in the absence and presence of TLR (Fig. 15.12B). This indicates reduced nitroxide motions. As the nitroxide was attached far away from the sites of interactions, no changes in τ_i/τ_B motions are expected, and reduced nitroxide motion report increased τ_R due to the formation of a higher molecular weight TL1/TLR complex (Fig. 15.12A). This provided the first direct evidence that the GAAA tetraloop can dock into an isolated receptor in solution.

Furthermore, spectra obtained in the presence of various TLR concentrations were analyzed using a spectral decomposition procedure (see an example in Fig. 15.12C). The normalized TL1-alone spectrum was scaled and subtracted from normalized "TL1 + TLR" spectra. At each TLR concentration, the fraction of unbound TL1 was represented by the largest possible scaling factor that gives a difference spectrum resembling an EPR spectrum with the lowest possible mobility. TLR concentration dependence of these fractions thus generates a binding curve, and gave a measured K_d of 0.4 m*M* between the GAAA tetraloop and its receptor (Fig. 15.12D). This is a weak interaction and is difficult to measure using other methods (Qin *et al.*, 2001).

This study highlights two important facets of using the τ_R effect. First, the nitroxide may be attached at a remote site and therefore will not perturb the native interaction. In addition, as an EPR experiment generally requires a nitroxide concentration greater than 10 μM, the method is suitable for measuring interactions where the K_d is approximately 10–1000 μM.

Acknowledgments

This research was supported by the National Institutes of Health (R01 GM069557, PZQ), Nation Science Foundation (MCB 054652, PZQ), and the Icelandic Research Fund (60028021, STS).

REFERENCES

Abakumov GA, Tikhonov VD. Reaction of stable radical 2,2,6,6-tetra-methylpiperidone-4-oxyl-1 with acids. Biol. Bull. Acad. Sci. USSR 1969:796–801.

Al-Hashimi HM, et al. Mg^{2+}-induced variations in the conformation and dynamics of HIV-1 TAR RNA probed using NMR residual dipolar couplings. J. Mol. Biol 2003;329:867–873. [PubMed: 12798678]

Altenbach C, et al. Structural studies on transmembrane proteins. 2. Spin labeling of bacteriorhodopsin mutants at unique cysteines. Biochemistry 1989;28:7806–7812. [PubMed: 2558712]

Barhate N, et al. A nucleoside that contains a rigid nitroxide spin label: A fluorophore in disguise. Angew. Chem. Int. Ed. Engl 2007;46:2655–2658. [PubMed: 17309085]

Blair DP, Sydenham PH. Phase sensitive detection as a means to recover signals buried in noise. J. Phys. E 1975;8:621–627.

Brodsky AS, Williamson JR. Solution structure of the HIV-2 TAR-argininamide complex. J. Mol. Biol 1997;267:624–639. [PubMed: 9126842]

Cantor, CR.; Schimmel, PR. Biophysical Chemistry. Vol. Vol. 2. San Francisco: W.H. Freeman; 1980. p. 460-564.

Cekan P, et al. Rigid spin-labeled nucleoside Ç: A nonperturbing EPR probe of nucleic acid conformation. Nucleic Acids Res 2008;36:5946–5954. [PubMed: 18805908]

Columbus L, Hubbell WL. A new spin on protein dynamics. Trends Biochem. Sci 2002;27:288–295. [PubMed: 12069788]

Columbus L, Hubbell WL. Mapping backbone dynamics in solution with site-directed spin labeling: GCN4–58 bZip free and bound to DNA. Biochemistry 2004;43:7273–7287. [PubMed: 15182173]

Columbus L, et al. Molecular motion of spin-labeled side chains in a-helices: Analysis by variation of side chain structure. Biochemistry 2001;40:3828–3846. [PubMed: 11300763]

Cova S, et al. Versatile digital lock-in detection technique: Application to spectrofluorometry and other fields. Rev. Sci. Instrum 1979;50:296. [PubMed: 18699495]

Edwards TE, Sigurdsson ST. Electron paramagnetic resonance dynamic signatures of TAR RNA—Small molecule complexes provide insight into RNA structure and recognition. Biochemistry 2002;41:14843–14847. [PubMed: 12475232]

Edwards TE, Sigurdsson ST. EPR spectroscopic analysis of TAR RNA-metal ion interactions. Biochem. Biophys. Res. Commun 2003;303:721–725. [PubMed: 12659878]

Edwards TE, Sigurdsson ST. Site-specific incorporation of nitroxide spin-labels into 2′-positions of nucleic acids. Nat. Protoc 2007;2:1954–1962. [PubMed: 17703207]

Edwards TE, et al. Site-specific incorporation of nitroxide spin-labels into internal sites of the TAR RNA: Structure-dependent dynamics of RNA by EPR spectroscopy. J. Am. Chem. Soc 2001;123:1527–1528. [PubMed: 11456739]

Edwards TE, et al. Investigation of RNA-protein and RNA-metal ion interactions by electron paramagnetic resonance spectroscopy. The HIV TAR–Tat motif. Chem. Biol 2002;9:699–706. [PubMed: 12079781]

Edwards TE, et al. Identification of amino acids that promote specific and rigid TAR RNA-tat protein complex formation. Chem. Biol 2005;12:329–337. [PubMed: 15797217]

Fajer, PG. Electron spin resonance spectroscopy labeling in proteins and peptides analysis. In: Meyers, R., editor. Encyclopedia of Analytical Chemistry. Chichester: Wiley; 2000. p. 5725-5761.

Fidanza JA, et al. Site-specific labeling of DNA-sequences containing phosphorothioate diesters. J. Am. Chem. Soc 1992;114:5509–5517.

Fischhaber PL, et al. Synthesis of duplex DNA containing a spin labeled analog of 2'-deoxycytidine. Nucleosides Nucleotides 1997;16:365–377.

Frankel AD. Activation of HIV transcription by Tat. Curr. Opin. Genet. Dev 1992;2:293–298. [PubMed: 1638124]

Gannett PM, et al. Probing triplex formation by EPR spectroscopy using a newly synthesized spin label for oligonucleotides. Nucleic Acids Res 2002;30:5328–5337. [PubMed: 12466559]

Grant GP, et al. Diastereomer characterizations of nitroxide-labeled nucleic acids. Biochem. Biophys. Res. Commun 2008;371:451–455. [PubMed: 18442474]

Grant GPG, et al. Motions of the substrate recognition duplex in a group I intron assessed by site-directed spin labeling. J. Am. Chem. Soc 2009;131:3136–3137. [PubMed: 19220053]

Hamy F, et al. Hydrogen-bonding contacts in the major groove are required for human immunodeficiency virus type-1 tat protein recognition of TAR RNA. J. Mol. Biol 1993;230:111–123. [PubMed: 8450529]

Hara H, et al. 4-Thiouridine-specific spin-labeling of *E. coli* transfer RNA. Biochem. Biophys. Res. Commun 1970;38:305–311. [PubMed: 4313932]

Hermann D. Spin-labeled nucleic acids. Acc. Chem. Res 1977;10:47–54.

Hustedt EJ, et al. Motions of short DNA duplexes: An analysis of DNA dynamics using an EPR-active probe. Biochemistry 1993;32:1774–1787. [PubMed: 8382521]

Keyes, RS.; Bobst, AM. Spin-labeled nucleic acids. In: Berliner, LJ., editor. Biological Magnetic Resonance. Vol. Vol. 14. New York: Plenum Press; 1998. p. 283-338.

Keyes RS, et al. Overall and internal dynamics of DNA as monitored by five-atom-tethered spin labels. Biophys. J 1997;72:282–290. [PubMed: 8994613]

Kim NK, et al. A distance ruler for RNA using EPR and site-directed spin-labeling. Chem. Biol 2004;11:939–948. [PubMed: 15271352]

Klug CS, Feix JB. Methods and applicants of site-directed spin labeling EPR spectroscopy. Methods Cell Biol 2008;84:617–658. [PubMed: 17964945]

Liang Z, et al. An electron spin resonance study of DNA dynamics using the slowly relaxing local structure model. J. Phys. Chem 2000;104:5372–5381.

Macosko JC, et al. A novel 5 displacement spin-labeling technique for electron paramagnetic resonance spectroscopy of RNA. RNA 1999;5:1158–1166. [PubMed: 10496217]

Marsh D. Electron spin resonance: Spin labels. Mol. Biol. Biochem. Biophys 1981;31:51–142. [PubMed: 6262623]

Mchaourab HS, et al. Motion of spin-labeled side chains in T4 lysozyme. Correlation with protein structure and dynamics. Biochemistry 1996;35:7692–7704. [PubMed: 8672470]

Miller TR, et al. A probe for sequence-dependent nucleic acid dynamics. J. Am. Chem. Soc 1995;117:9377–9378.

Nagahara S, et al. Spin-labeled oligonucleotides site specifically labeled at the internucleotide linkage—Separation of stereoisomeric probes and EPR spectroscopical detection of hybrid formation in solution. Nucleosides Nucleotides 1992;11:889–901.

Okamoto A, et al. Nitroxide-labeled guanine as an ESR spin probe for structural study of DNA. Bioorg. Med. Chem 2004;14:3415–3418.

Piton N, et al. Base-specific spin-labeling of RNA for structure determination. Nucleic Acids Res 2007:3128–3143. [PubMed: 17452362]

Poole, CP. Electron spin resonance: A comprehensive treatise on experimental techniques. Mineola, NY: Dover Publications, Inc.; 1996.

Prisner T, et al. Pulsed EPR spectroscopy: Biological applications. Annu. Rev. Phys. Chem 2001;52:279–313. [PubMed: 11326067]

Qin PZ, et al. Quantitative analysis of the isolated GAAA tetraloop/receptor interaction in solution: A site-directed spin-labeling study. Biochemistry 2001;40:6929–6936. [PubMed: 11389608]

Qin PZ, et al. Monitoring RNA base structure and dynamics using site-directed spin-labeling. Biochemistry 2003;42:6772–6783. [PubMed: 12779332]

Qin PZ, et al. A model system for investigating lineshape/structure correlations in RNA site-directed spin labeling. Biochem. Biophys. Res. Commun 2006;343:117–124. [PubMed: 16530169]

Qin PZ, et al. Measuring nanometer distances in nucleic acids using a sequence-independent nitroxide probe. Nat. Protoc 2007;2:2354–2365. [PubMed: 17947978]

Roy S, et al. A bulge structure in HIV-1 TAR RNA is required for Tat binding and Tat-mediated trans-activation. Genes Dev 1990;4:1365–1373. [PubMed: 2227414]

Schiemann O, et al. A PELDOR-based nanometer distance ruler for oligonucleotides. J. Am. Chem. Soc 2004;126:5722–5729. [PubMed: 15125665]

Schiemann O, et al. Spin-labeling of oligonucleotides with the nitroxide TPA and use of PELDOR, a pulse EPR method, to measure intramolecular distances. Nat. Protoc 2007;2:904–923. [PubMed: 17446891]

Schneider, DJ.; Freed, JH. Calculating slow motional magnetic resonance spectra: A user's guide. In: Berliner, LJ., editor. Spin Labeling: Theory and Applications. Vol. Vol. 3. New York: Plenum Press; 1989. p. 1-76.

Sowa GZ, Qin PZ. Site-directed spin labeling studies on nucleic acid structure and dynamics. Prog. Nucleic Acid Res. Mol. Biol 2008;82:147–197. [PubMed: 18929141]

Spaltenstein A, et al. A rigid and nonperturbing probe for duplex DNA motion. J. Am. Chem. Soc 1988;110:1299–1301.

Varani L, et al. Structure of tau exon 10 splicing regulatory element RNA and destabilization by mutations of frontotemporal dementia and parkinsonism linked to chromosome 17. Proc. Natl. Acad. Sci. USA 1999;96:8229–8234. [PubMed: 10393977]

Xi X, et al. HIV-1 nucleocapsid protein NCp7 and its RNA stem loop 3 partner: Rotational dynamics of spin-labeled RNA stem loop. Biochemistry 2008;47:10099–10110. [PubMed: 18729386]

Zhang Z, et al. Rotational dynamics of HIV-1 nucleocapsid protein NCp7 as probed by a spin label attached by peptide synthesis. Biopolymers 2008;89:1125–1135. [PubMed: 18690667]

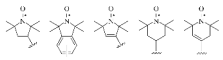

Figure 15.1.
Structures of nitroxides that have been used for spin-labeling.

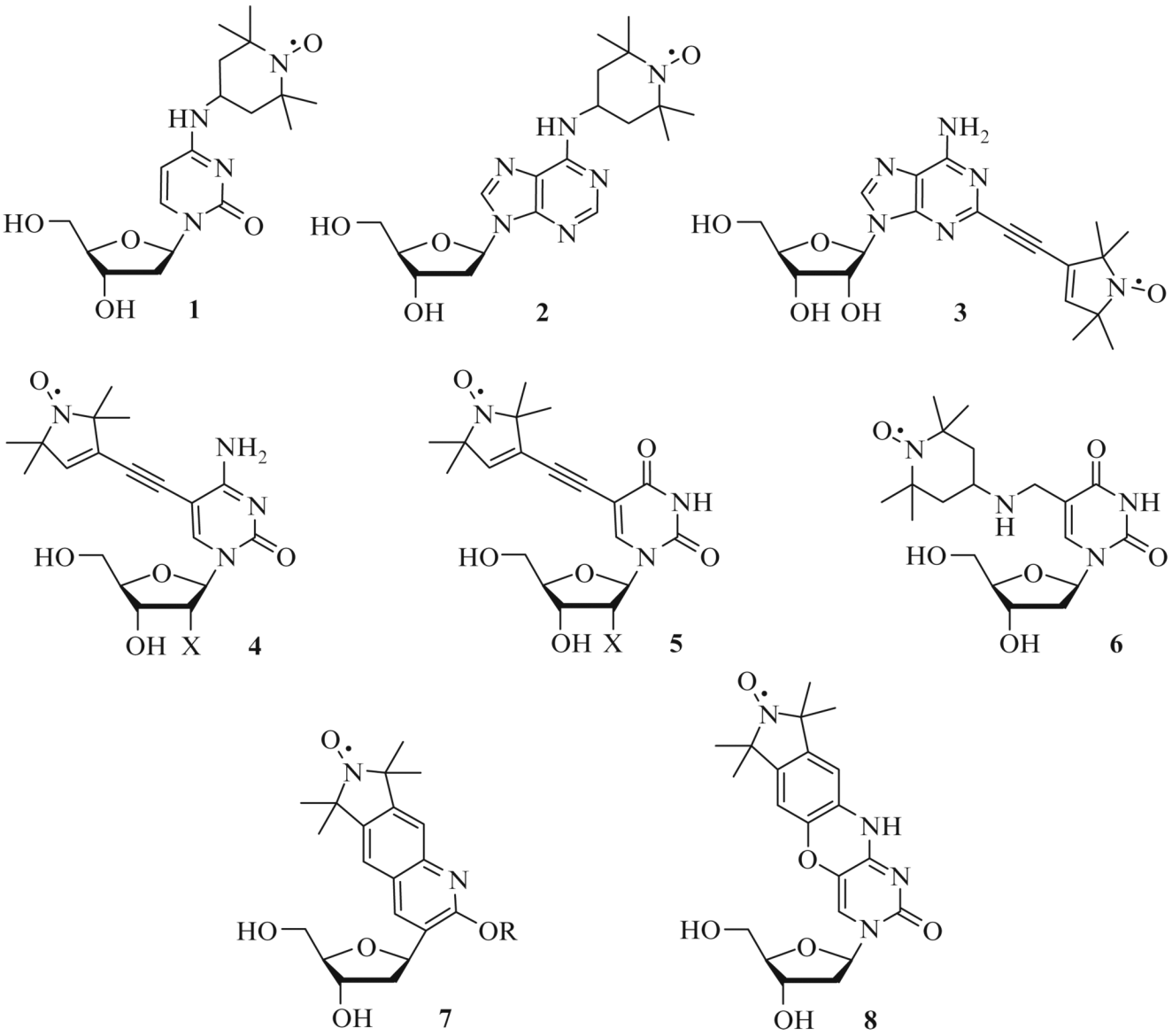

Figure 15.2.
Spin-labeled nucleosides that have been incorporated into nucleic acids during chemical synthesis of the oligomer. In structures **4** and **5**, X is either H or OH.

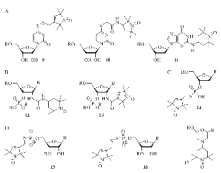

Figure 15.3.
Nucleotides that have been spin-labeled by postsynthetic modification of the oligomer at either the base (A), the sugar (B), the internal phosphodiester (C), or the terminus (D). “B” indicates the nucleoside base.

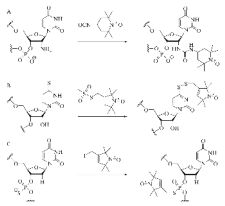

Figure 15.4.
Postsynthetic labeling of internal nucleotides in RNA. (A) Reaction of a nitroxide containing an aliphatic isocyanate with 2′-amino groups in RNA. (B) Reaction of methanethiosulfonate nitroxide with a 4-thiouridine nucleotide in RNA. (C) Reaction of iodomethyl nitroxide with deoxyribo-phosphorothiolate linkage in RNA.

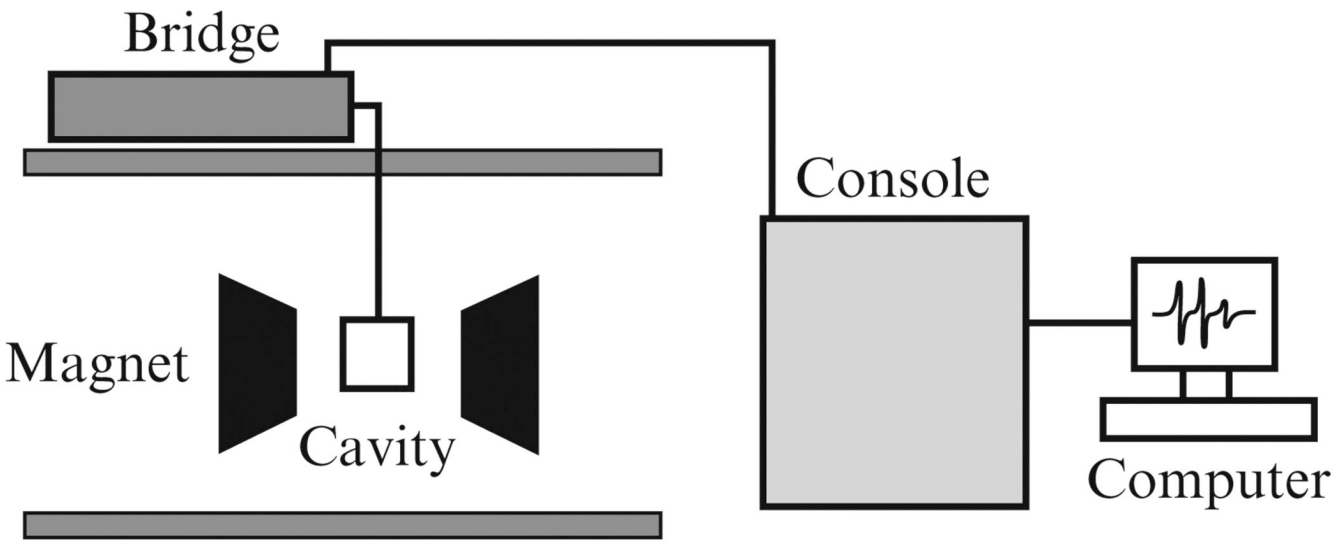

Figure 15.5.
The general layout of an EPR spectrometer. The spectrometer consists of a microwave bridge, a cavity (or resonator), magnets, and a console. The microwave bridge houses the microwave source and the detector, together with other control and support components. The cavity is where resonance between the electron spins and the electromagnetic radiation takes place, and is stationed between the magnets. The console contains signal processing units and electronics that control the operation of the bridge. The console is generally connected to a computer for spectral acquisition and data analysis.

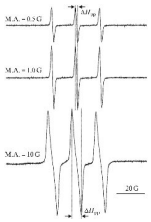

Figure 15.6.

Effects of modulation amplitude on cw-EPR line-shape. Spectra shown were obtained on a Bruker EMX spectrometer equipped with a high-sensitive cavity. The sample was an aqueous solution of tempol (4-hydroxy-2,2,6,6-tetramethylpiperidine-1-oxyl) (12.5 μM, 5 μl) placed in a round glass capillary (0.6 mm ID, 0.8 mm OD; Vitrocom, Inc., Mountain Lakes, NJ) sealed at one end. Acquisition parameters listed in Table 15.1 were used, except that the modulation amplitude (M.A.) was varied as respectively indicated for each spectrum. Note that these spectra have not been normalized, and differences in the amplitude of the spectrum are due to the different modulation amplitudes used.

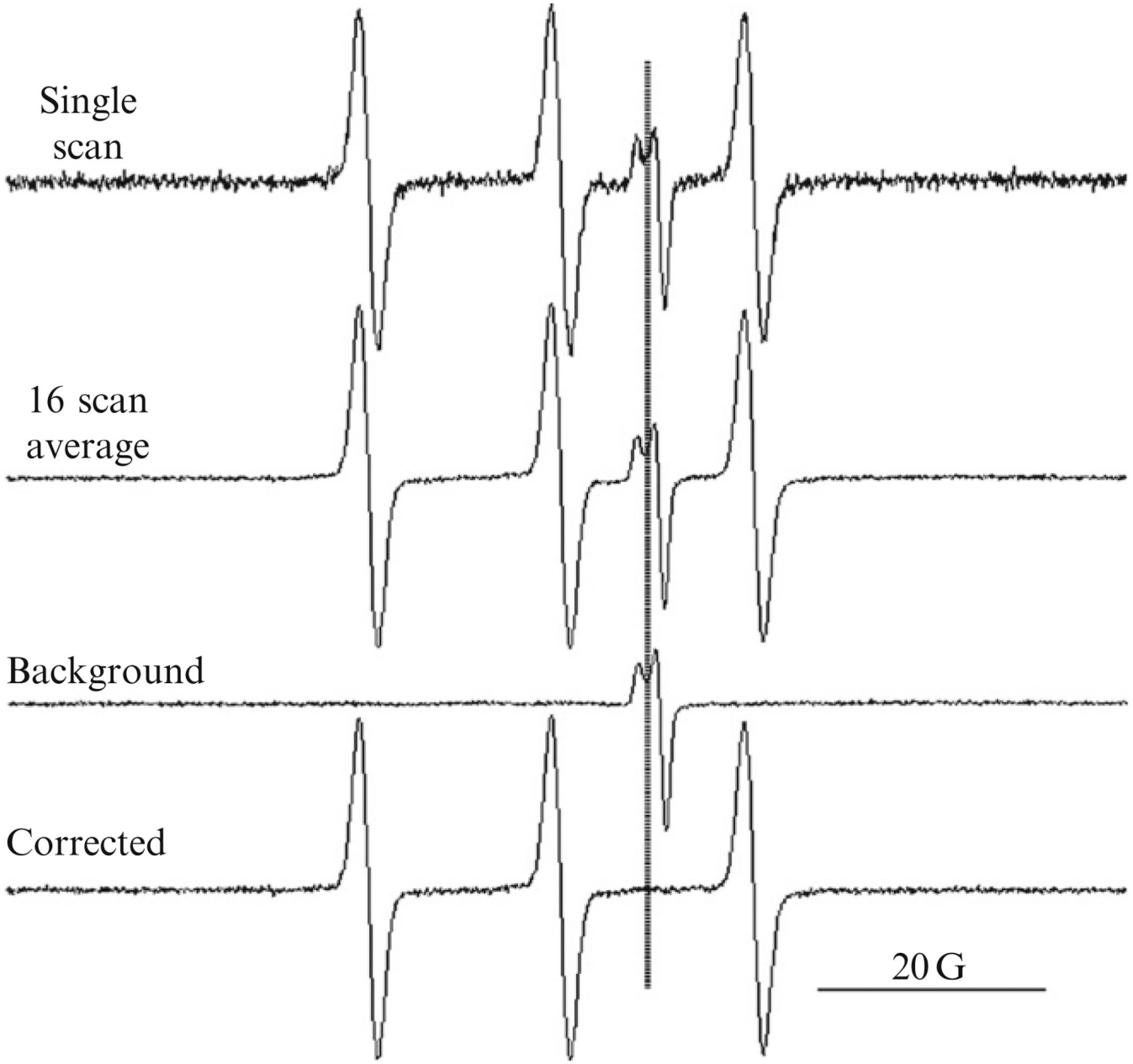

Figure 15.7.
Examples of spectral processing. Acquisition parameters listed in Table 15.1 were used to measure a solution of tempol. The background spectrum was collected using water, which shows a feature due to a cavity defect.

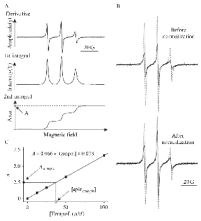

Figure 15.8.

Examples of spectral integration and normalization. Spectra shown were obtained with nitroxide label **14** (Fig. 15.3C). Acquisition parameters are listed in Table 15.1, except that number of scans = 4 and number of points = 1024. (A) Spectrum of an aqueous sample of a 23-nt RNA, together with its 1st and 2nd integrals. (B) Spectral comparison between a 23-nt RNA (40 μM, dotted line) and a 49-nt RNA (30 μM, solid line). Comparison of the normalized spectra is not skewed by the different amount of labeled RNAs used in the measurement, and reports different nitroxide behavior due primarily to the difference in RNA size. (C) An example of spin counting. The calibration curve was generated by linear fitting (solid line) of data points (solid square) obtained using tempol solutions of various concentrations. Using this calibration curve, the sample measured in (A) was found to contain 37.5 μM of spins ($A_{\text{sample}} = 2.5$). Based on an RNA concentration of 40 μM, the nitroxide labeling efficiency was determined to be 93.6%.

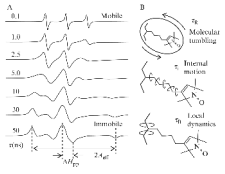

Figure 15.9.

Nitroxide dynamics and cw-EPR spectral line-shape. (A) Simulated X-band EPR spectra of nitroxides undergoing isotropic rotation at different rotational correlation time τ. (B) The three modes of motion that contribute to nitroxide dynamics. Adopted from Sowa and Qin (2008) with permission.

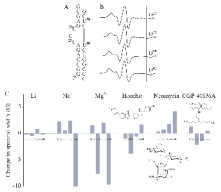

Figure 15.10.
(A) The TAR RNA construct used in this study. Spin-labeled nucleotides are shown in bold. (B) EPR spectra of spin-labeled TAR RNA samples (Edwards *et al*., 2001). The position of the spin label is indicated on each spectrum. The samples were prepared in 50% sucrose/100 m*M* NaCl, 10 m*M* sodium phosphate, 0.1 μM Na_2EDTA, pH 7.0. A line indicating the spectral width of U23 TAR RNA is extended through the other spectra, to allow for visual qualitative comparison of the EPR spectral widths. (C) Changes in EPR spectral width plotted as a function of spin-labeled position (U23, U25, U38, and U40) to give a dynamic signature for each metal ion and small molecule that binds to the TAR RNA (Edwards and Sigurdsson, 2002, 2003). Chemical structures of Hoechst, CGP 40336A, and neomycin are shown.

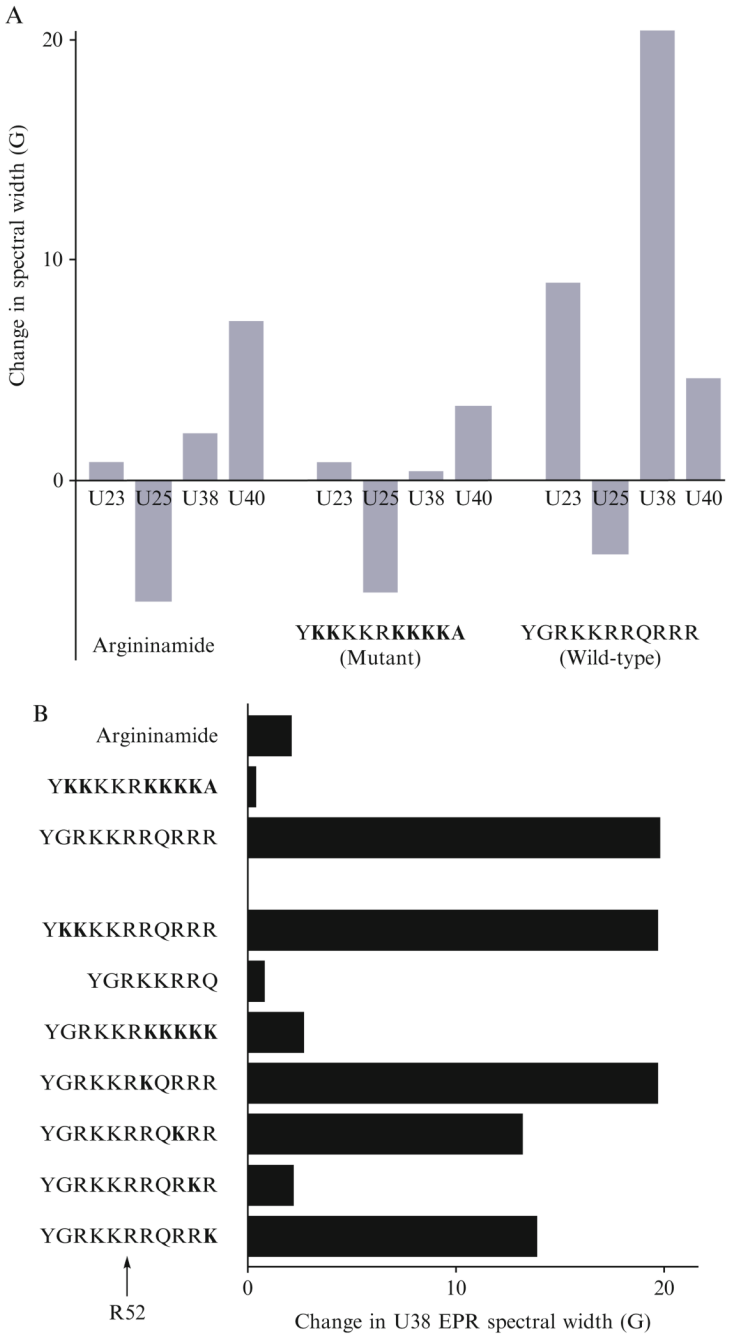

Figure 15.11.

(A) Dynamic signatures of argininamide and two Tat-derived peptides, the wild-type sequence, and a mutant. (B) Sequences of the Tat-derived peptides and changes in EPR spectral width of U38 in the presence of each peptide. Amino acid mutations are shown in bold. Arrow shows the location of the essential R52 in the peptide sequence.

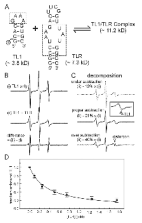

Figure 15.12.
SDSL studies of GAAA tetraloop binding to its RNA receptor. (A) Schematics of the experimental design, with R indicating the nitroxide label. (B) Normalized TL1 EPR spectra obtained in the absence (i) and presence (ii) of TLR (1.75 m*M*). Due to weak binding, the "TL1 + TLR" spectrum is a composite of the unbound TL1 and the complex. (C) Spectral decomposition by subtracting scaled TL1 spectrum from that of "TL1 + TLR." The value used for properly subtraction (middle, 21%) represents the fraction of unbound TL1 in the presence of 1.75 m*M* TLR. If the scaling factor is too small (top, under subtraction), the resulting spectrum shows remaining features of the free TL1, which is most clearly observed by comparing the low-field regions between the under subtracted spectrum (dotted line) and the properly subtracted spectrum (solid line) (see inset). In the opposite case (bottom, over subtraction), the resulting spectrum (dash line) is distorted (indicated by the triangle). (D) Binding curve between TL1 and TLR. Data reproduced from Qin *et al*. (2001) with permission.

Table 15.1

Examples of acquisition parameters used with a Bruker EMX spectrometer

Parameter	Sample value	Trouble-shooting notes
Center field	3324 G	Section 2.3.1.2
Scan width	100 G	Section 2.3.1.2
Microwave power	2 mW (20 dB)	Section 2.3.2.2
Modulation amplitude	1 G	Section 2.3.2.1
Modulation frequency	100 kHz	Section 2.3.2.1
Modulation phase	42°	Section 2.3.1.3
Number of points	2048	Section 2.3.2.3
Conversion time	40.96 ms	Section 2.3.2.3
Time constant	20.48 ms	Section 2.3.2.3
Number of scans	16	Section 2.3.1.5
Receiver gain	6.3×10^3	Section 2.3.1.4